IMU LAB4 REPORT

Driver Files uploaded by: patil.tap@northeastern.edu (Tapan Patil)

Introduction

This lab focuses on evaluating sensor technologies for navigation by analyzing data from a vehicle equipped with GPS and an Inertial Measurement Unit (IMU). We collected two datasets: one during circular driving and another from a tour around Boston. The goal is to assess the performance of the VN-100 IMU and a USB-based GNSS puck in estimating vehicle heading, forward velocity, and trajectory through sensor fusion techniques. We will calibrate the magnetometer and compare yaw estimates from both the IMU and magnetometer to enhance navigational accuracy. Additionally, we will integrate acceleration data to estimate forward velocity and displacement, providing a comprehensive analysis of the vehicle's movement. This report details our methods, findings, and observations from the collected datasets.

Methodology

Data Collection

Car Donuts Experiment:

- A rosbag was recorded, titled **data_going_in_circles**.
- The vehicle was maneuvered in a circular path for roughly 4 to 5 laps, with an emphasis on sustaining a uniform circular motion to facilitate accurate data gathering.
- The rosbag recording concluded after the laps were completed, while the car and ROS2 drivers continued to operate.

Mini Boston Tour:

- A second rosbag named **data_driving** was initiated.
- The vehicle was navigated around Boston, covering a distance of at least 2 to 3 kilometers with few turns along the way.
- Upon returning to the starting location, the rosbag recording was stopped, and the car along with the ROS2 drivers was powered down.

Data Analysis

Heading (Yaw) Estimation

To accurately estimate the heading, the first focus was on calibrating the magnetometer readings to account for both "hard-iron" and "soft-iron" distortions while the device is in motion.

Distortion Types

Hard-iron Distortions: These are caused by permanent magnetic fields from nearby ferromagnetic objects. Such distortions can significantly affect the accuracy of magnetic readings, leading to erroneous heading estimations.

For hard-iron correction, the offset is calculated using the formula:

$$Hard\ iron\ offset\ =\ (max(Mx)\ +\ min(Mx))\ /\ 2, (max(My)\ +\ min(My))\ /\ 2$$

This offset is then subtracted from the raw magnetic data:

$$Mcorrected\ =\ Mraw\ -\ hardironoffset$$

Soft-iron Distortions: These arise from materials that become magnetized in the presence of an external magnetic field. They distort the magnetic field lines, thereby affecting the readings taken by the magnetometer.

For soft-iron correction, the covariance matrix of the corrected data is used to derive the soft-iron correction matrix:

$$soft\ iron\ matrix = V \cdot inv(diag(eig\ val)$$

The covariance calculation method for soft-iron correction involves assessing the relationship between the x and y components of the magnetic field data. By computing the covariance matrix from the corrected magnetic readings, we capture how these components vary together. Each entry in the matrix reflects the degree to which the changes in one component correspond to changes in the other. The covariance matrix then facilitates the derivation of eigenvalues and eigenvectors, which are used to create a soft-iron correction matrix, effectively compensating for these distortions and improving the accuracy of the magnetic data.

The plot below illustrates the magnetometer data before and after the Hard and Soft iron correction.

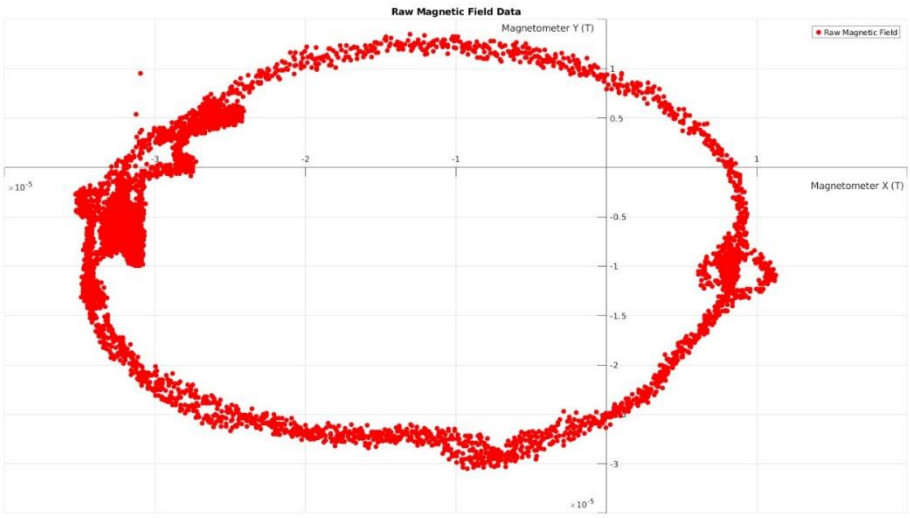

Figure 1. Raw Magnetic Data (data_going_in_circles)

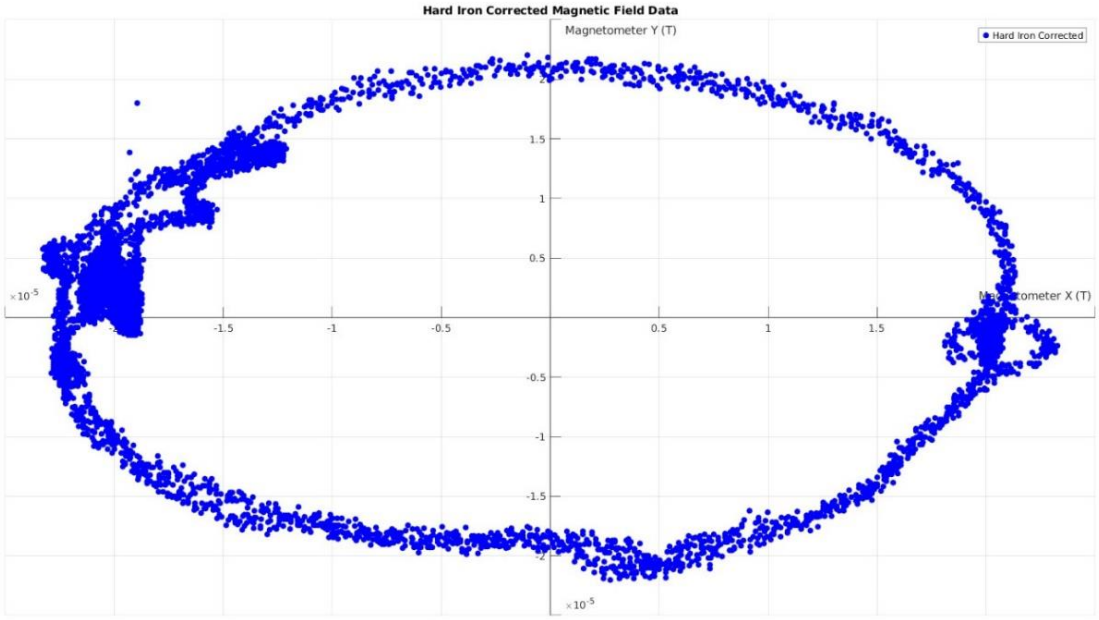

Figure 2. Hard Iron Correction on Raw Magnetic Data

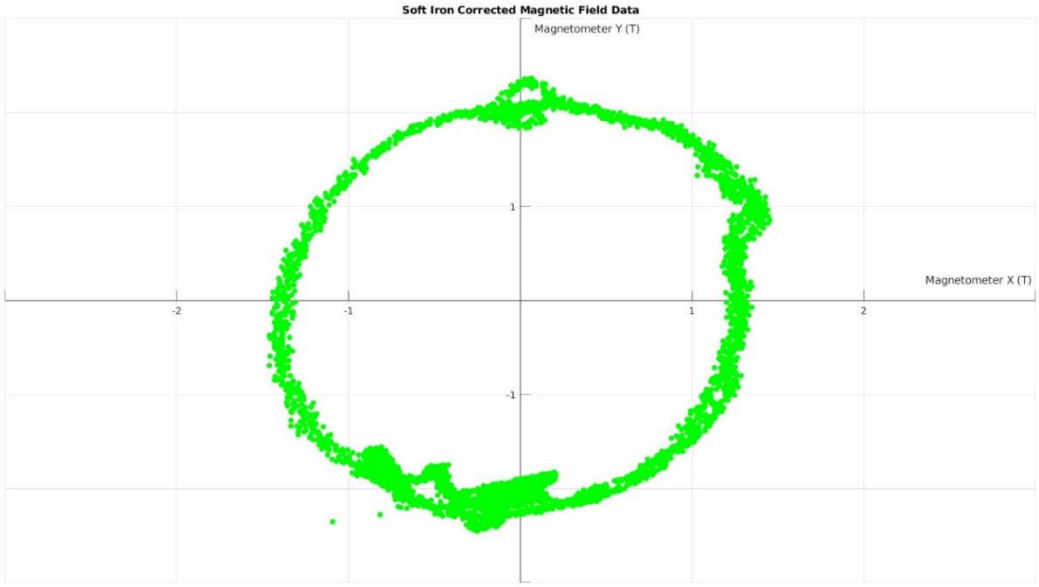

Figure 3. Soft Iron Correction on Raw Magnetic Data

Sensor Fusion

Raw Magnetic Yaw vs Corrected Magnetic Yaw

Further analysis was performed using data from the data_driving ROS bag, applying the previously obtained calibration technique for magnetometer correction on the data_going_in_circles ROS bag. Parameters calculated during the plotting are:

- Hard Iron Offset:

$$\begin{matrix} \text{X: } -22.0500 \\ \text{Y: } -62.6000 \end{matrix}$$

- Soft Iron Matrix:

$$\begin{bmatrix} 0.0059 & 0.0010 \\ 0.0010 & 0.0096 \end{bmatrix}$$

Following comparison plot visualizes the raw magnetometer yaw and the corrected yaw to assess the calibration's impact.

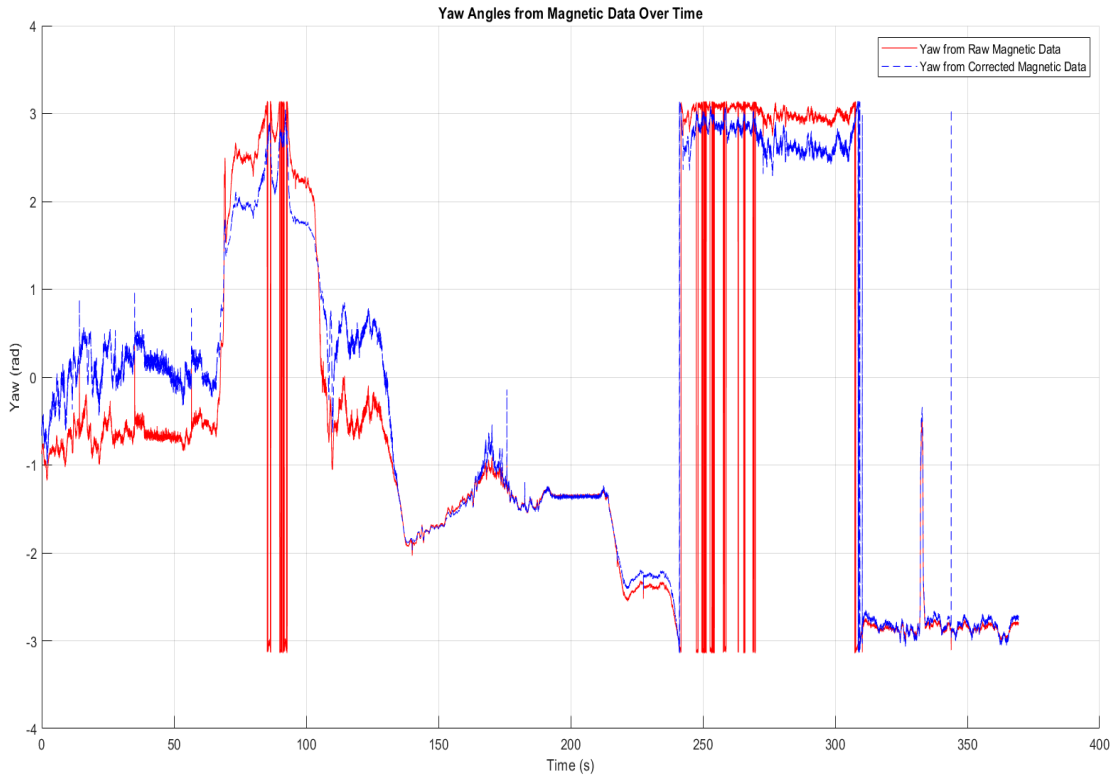

Figure 4. Comparison of Raw Magnetic and Corrected Magnetic Data (*data-driving*)

Corrected Magnetometer Yaw vs Gyro Integrated Yaw

To derive the yaw angle, the yaw rate from the gyroscope was integrated using the cumtrapz commands in MATLAB. The formula given ahead summarizes the calculation of yaw angle.

$$\theta_{yaw} = \int \omega_{yaw}\, dt$$

Where:

θ_{yaw} is the yaw angle.

ω_{yaw} is the yaw rate measured by the gyroscope.

The yaw angles obtained from the magnetometer and the yaw integrated from the gyroscope were plotted as below:

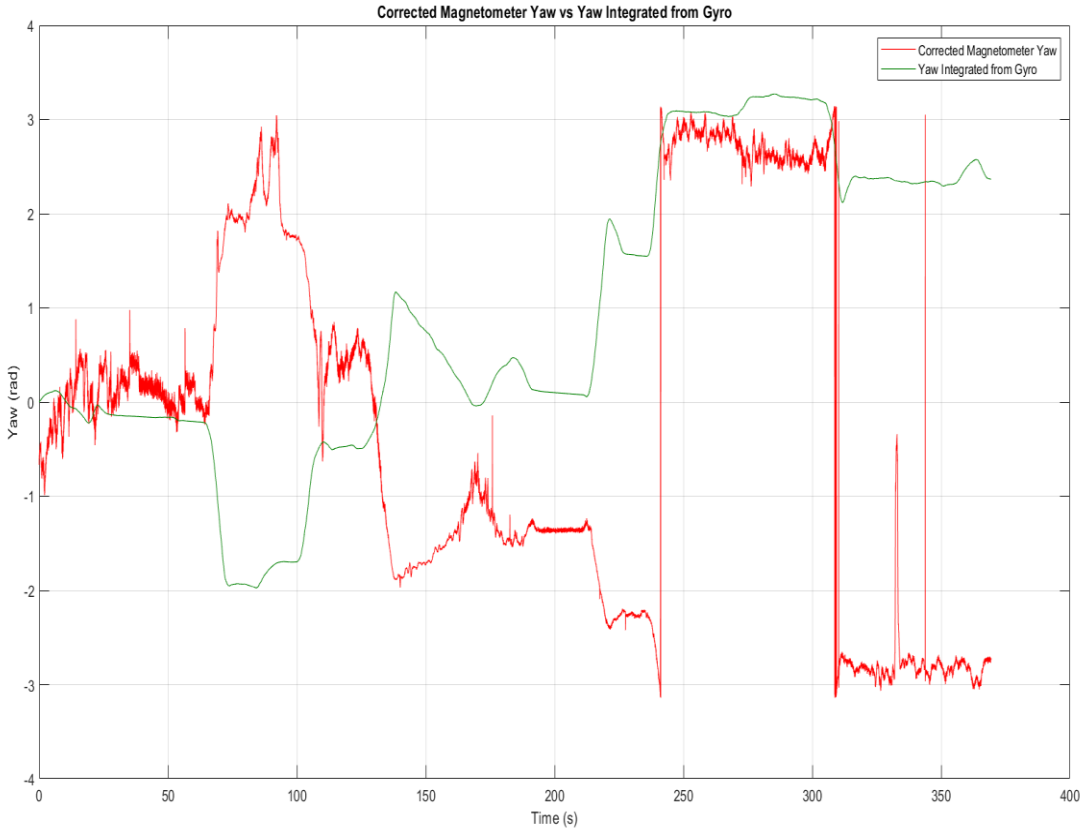

Figure 5. Corrected Magnetometer Yaw vs Gyro Integrated Yaw

Low Pass Filter, High Pass Filter, Complementary Filter

A low-pass filter is applied to the magnetometer yaw data, which serves to smooth out high-frequency noise and rapid fluctuations, providing a clearer representation of the overall orientation trend. This filtering is significant as magnetometer readings can be influenced by environmental disturbances, making them less reliable for detecting quick changes in orientation. On the other hand, a high-pass filter is utilized on the integrated yaw data from the gyroscope. This filter effectively removes low-frequency components, such as drift, that can accumulate over time. While gyroscopes excel at detecting rapid changes, they are susceptible to drift, which can lead to inaccuracies in long-term measurements.

By employing a complementary filter that combines the outputs of both filtering processes, we leverage the strengths of each sensor. The low-pass filter stabilizes the magnetometer data, providing reliable absolute orientation, while the high-pass filter captures the quick movements detected by the gyroscope, compensating for drift. This integrated approach results in a more accurate and robust yaw estimate. The complementary filter can be expressed as follows:

$$\theta comp = \alpha * \theta gyro + (1 - \alpha) * \theta mag$$

Where:

$\theta comp$ is the combined yaw estimate,
$\theta gyro$ is the yaw angle from the gyroscope,
θmag is the yaw angle from the magnetometer,
α is the filter coefficient (α = 0.93 used).

The filter coefficient α = 0.93 indicates that the estimate relies more heavily on the gyroscope data (93%, higher cutoff frequency for gyro) than the magnetometer data (7%). Gyroscopes are known for their ability to detect rapid angular changes with high accuracy over short time periods. By heavily weighting the gyroscope data (93%), the filter preserves this characteristic, allowing the combined estimate to respond quickly to sudden orientation changes especially for precise orientation along turns.

Cutoff Frequency Calculation:

$$fc = (1 - \alpha) / (2\pi * dt)$$

Where: α is the filter coefficient (0.93 in this case), dt is the sampling time interval. Based on 40 Hz output rate of IMU, the cutoff frequency comes out to be around 1.13 Hz.

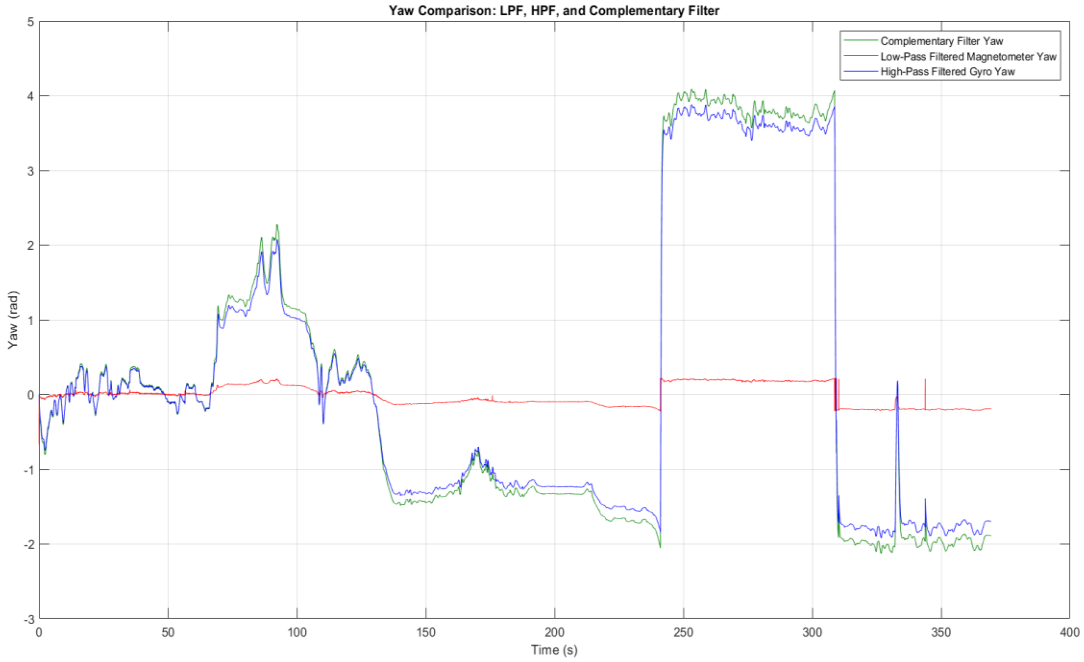

Figure 6. Comparison of Magnetometer Yaw (Low Pass Filtered), Gyro Integrated Yaw (High Pass Filtered) and Sensor Fusion Yaw (Complementary Filtered)

Furthermore, the comparison between sensor fusion yaw derived from the complementary filter, with the IMU yaw reveals the effectiveness of integrating multiple data sources.

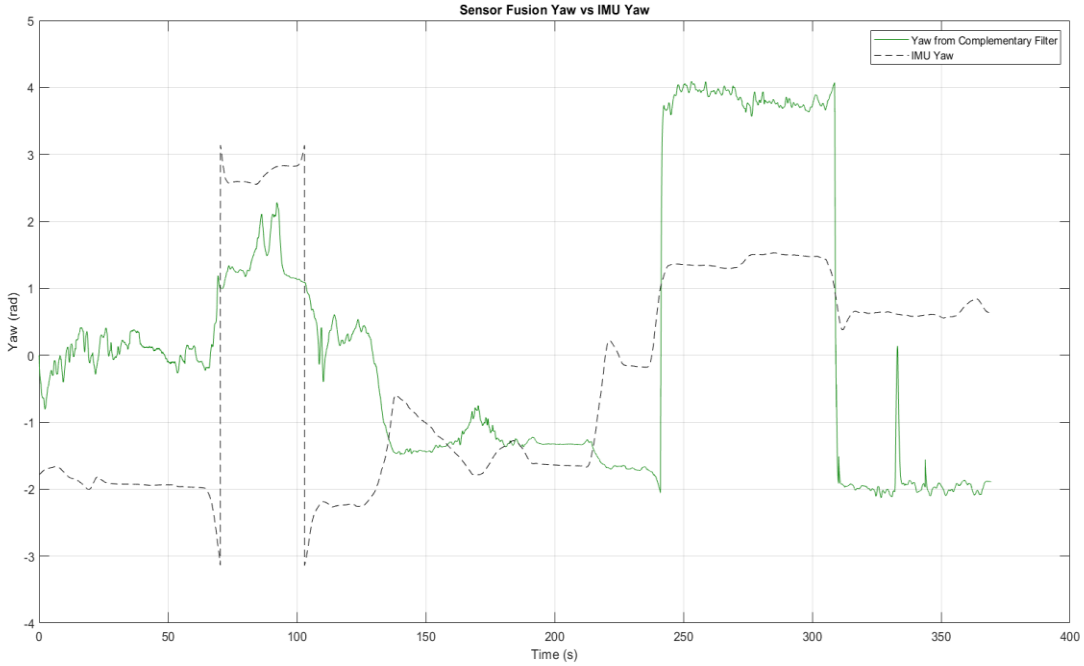

Figure 7. Comparison of Sensor Fusion Yaw and IMU Yaw

Based on the plots observed, I would prefer the Complementary Filter Yaw as it combines the rapid response of the gyroscope with the long-term stability of the magnetometer, providing a balanced and robust yaw estimate that can handle both quick maneuvers and extended driving periods and a similar pattern as observed with the IMU Yaw.

Forward Velocity Estimation

In this analysis, forward velocity estimates were calculated using both IMU acceleration data and GPS measurements. GPS velocity estimates were calculated by measuring the distance between consecutive GPS coordinates and dividing by the time intervals, providing a reliable assessment of actual movement and IMU velocity was obtained by integrating IMU acceleration. Both GPS and IMU velocities were then plotted to facilitate a visual comparison of the estimates. The following equations represent formulas used for gps velocity calculation.

$$distance(i) = sqrt((utm\ easting(i+1) - utm\ easting(i))\text{^}2 + (utm\ northing(i+1) - utm\ northing(i))\text{^}2)$$

$$gps\ velocity(i) = distance(i)\ /\ delta\_t$$

Before Adjustment: The initial plot (Figure 8.) indicated that the integrated velocity from the accelerometer displayed a positive slope. This was unexpected, as it suggested ongoing acceleration despite the presence of drops in velocity due to factors like red traffic lights, stop signs, and pedestrians crossing the road. There was no such acceleration to justify this positive slope, highlighting inaccuracies in the IMU data. This discrepancy was likely due to cumulative integration errors, sensor biases, and the IMU's sensitivity to noise and vibrations.To address this issue, a series of corrections were applied to the IMU acceleration data. This included the bias correction to eliminate unnecessary artifacts, the removal of fixed offsets to reduce sensor inaccuracies, and filtering out low values set to zero to eliminate high-frequency noise.

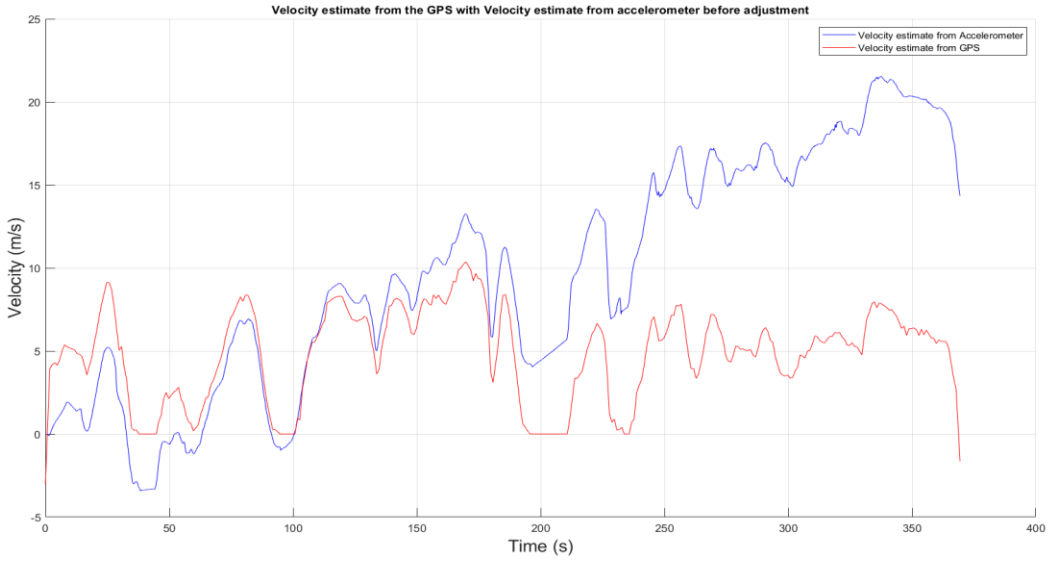

Figure 8. Velocity estimate from the GPS with Velocity estimate from accelerometer before adjustment

After Adjustment: Figure 9. represents a time series comparison of corrected estimated velocity (in m/s) from GPS and IMU, demonstrating the effectiveness of the adjustments made.

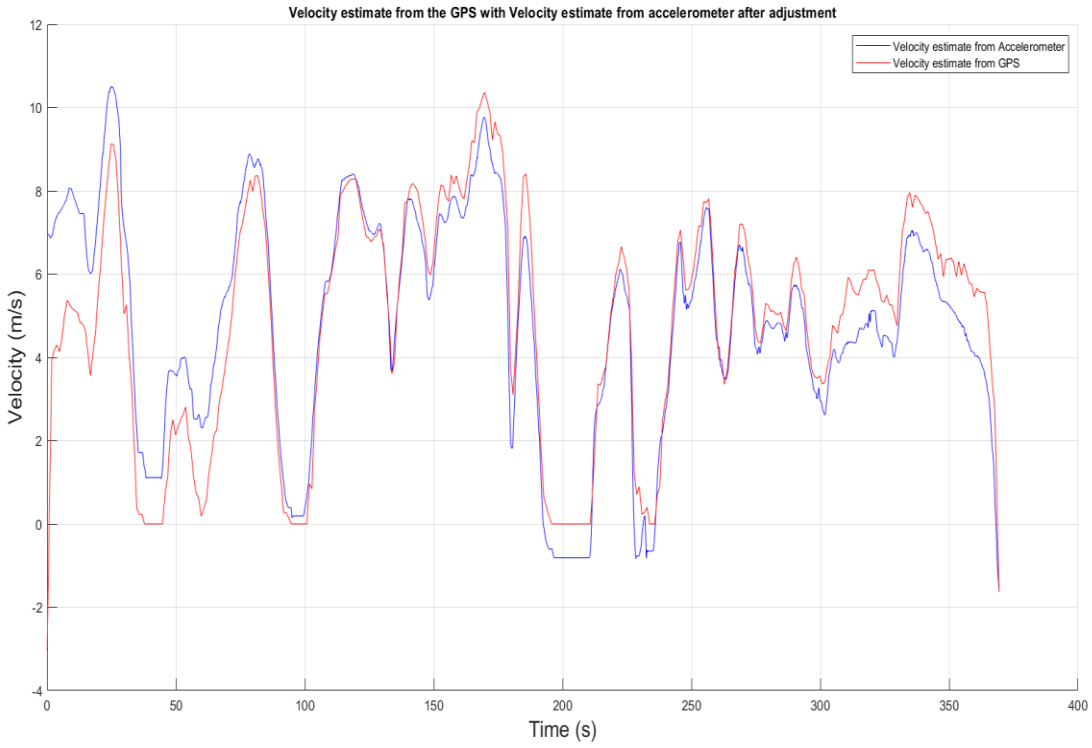

Figure 9. Velocity estimate from the GPS with Velocity estimate from accelerometer after adjustment

Dead Reckoning with IMU

In this analysis, dead reckoning was conducted in the lab using IMU data to estimate vehicle displacement, which was then compared to GPS-derived displacement (Figure 12).

Integration of Forward Velocity: The analysis began with the integration of forward velocity to obtain the vehicle's displacement in a two-dimensional plane.

Acceleration Components During Turns: As the data was recorded in a driving vehicle, several turns were encountered along the route. During turns, three acceleration components are ideally considered for dead reckoning.

- Forward acceleration (along axis)
- Outward acceleration due to inertia (skidding)
- Centripetal acceleration (due to difference in position of center of mass of vehicle and imu)

$$X\,(obs) = X\,ddot - \omega * Y\,dot - \omega\text{^}2 * xc$$

$$Y\,(obs) = Y\,ddot + \omega * X\,dot + \omega\,dot * xc$$

To simplify the analysis, the following assumptions were made in the lab:

- Zero Skidding: It was assumed that the vehicle did not shift sideways ($\dot{Y} = 0$).
- Centripetal Acceleration: This term was disregarded by setting the IMU's position relative to the vehicle's center of mass ($x_c = 0$), allowing focus on forward acceleration.

We get,

$$X\ (obs)\ =\ X\ ddot$$
$$Y\ (obs)\ =\ \omega\ *\ X\ dot$$

Y-Axis Acceleration: In the analysis, Y-Axis acceleration was assessed, where the only relevant component, based on the assumptions, was lateral acceleration ($\omega * X_dot$). The simplification that the center of mass and the center of rotation coincided was acknowledged, enabling the neglect of additional terms.

Velocity Calculation: Observed acceleration was integrated to derive forward velocity ($\dot{X}$). Subsequently, $\omega\dot{X}$ was computed and compared with the observed Y-axis acceleration from the IMU ($\ddot{y}obs$). Despite the overall pattern similarity, there were noticeable discrepancies in the signal's smoothness and noise levels. To address this, a Butterworth low-pass filter (cutoff frequency of 1.2 Hz) was applied to the Y-axis acceleration from the IMU. This filter helps preserve the signal's integrity while effectively attenuating higher-frequency noise. Figure 10 and Figure 11 demonstrate the comparison between two.

Heading Adjustment: The yaw angle from gyro rate integration, calculated previously in the lab, was utilized to rotate the estimated forward velocity into Easting (ve) and Northing (vn) components. This adjustment ensured that the trajectory accounted for the vehicle's orientation during movement.

Trajectory Estimation: Velocity components were integrated to estimate the vehicle's trajectory (xe, xn). The IMU-derived trajectory was then adjusted to align with the GPS track. This adjustment involved applying a scaling factor of 0.65 to both easting and northing components.

The following figures visualize the analysis done in Dead Reckoning of IMU section of lab.

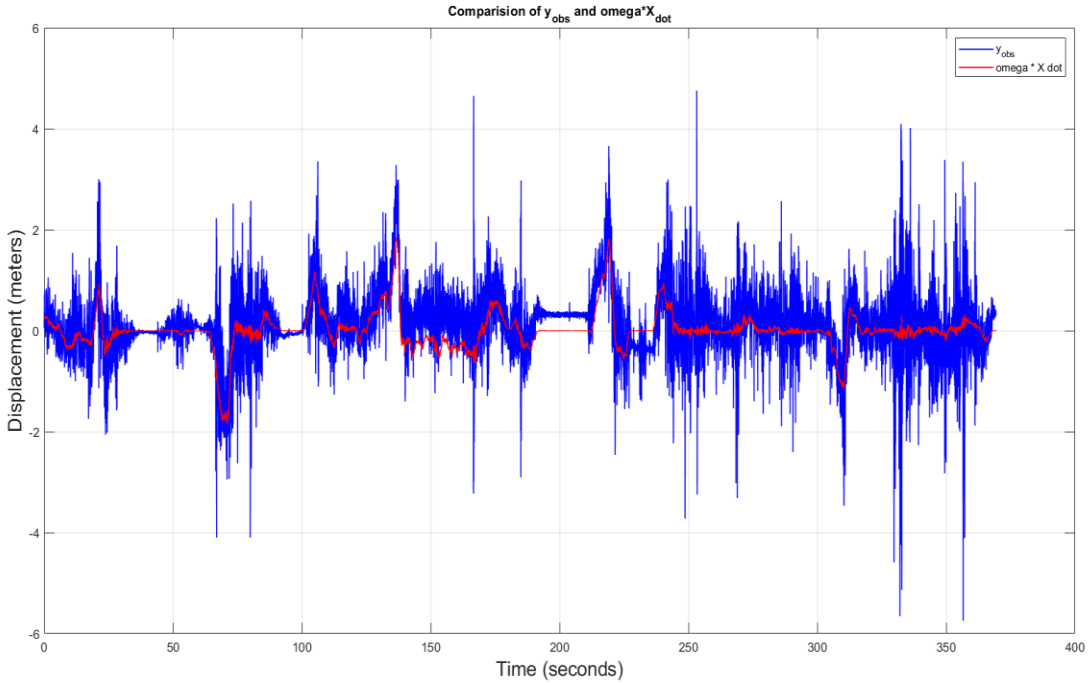

Figure 10. Comparison of Yobs (IMU linear acceleration Y) and wXdot

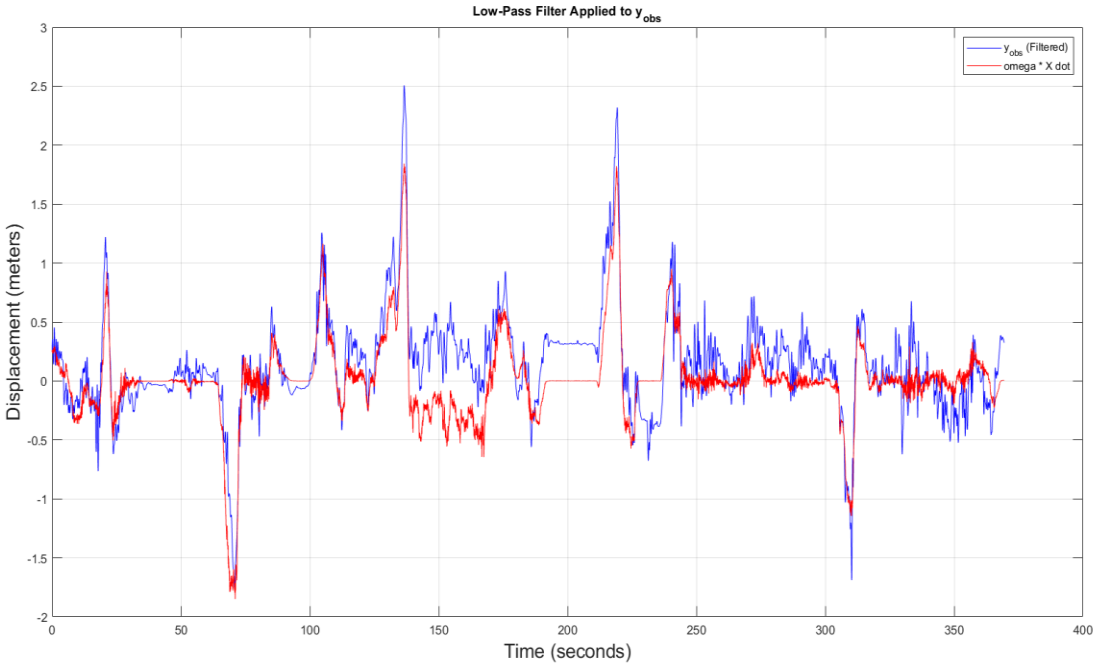

Figure 11. Comparison of Filtered Yobs (IMU linear acceleration Y) and wXdot

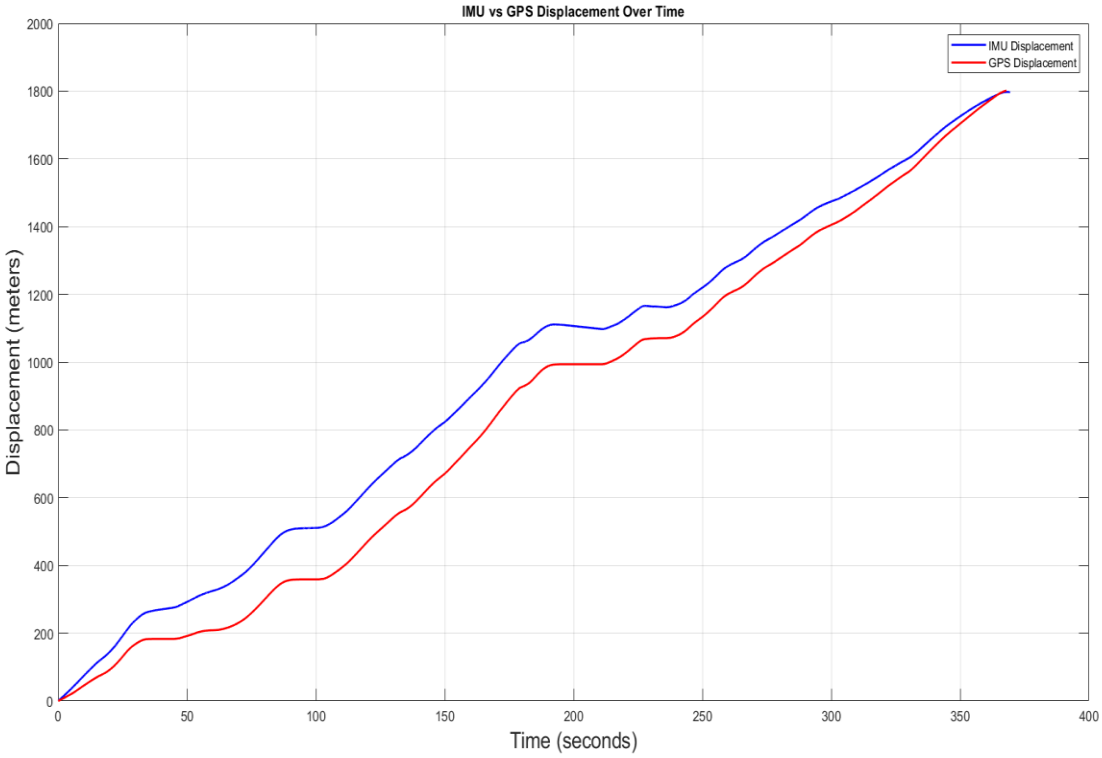

Figure 12. Comparison of IMU Displacement and GPS Displacement

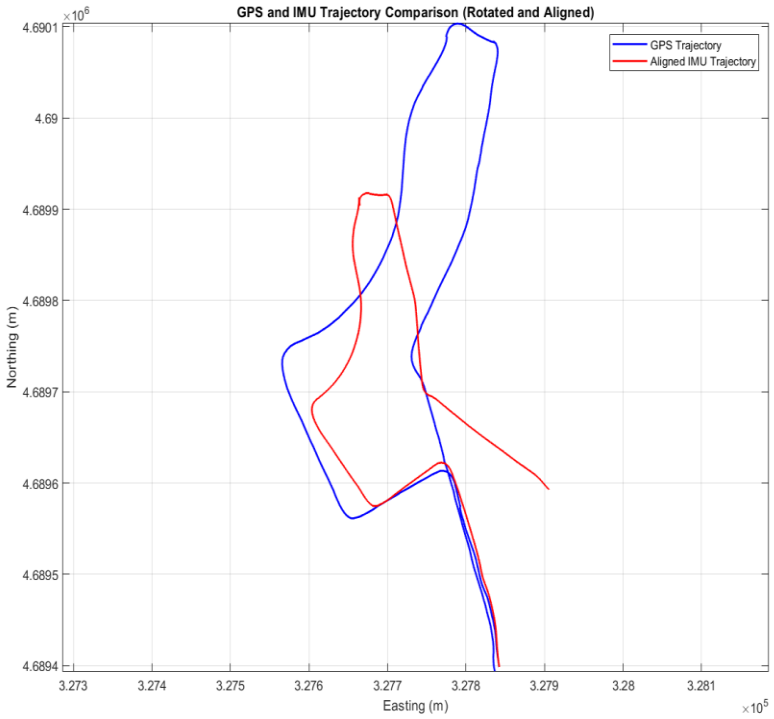

Figure 13. Comparison of GPS and IMU Trajectory